A Temperature-Aware Large-Signal SPICE Model for Depletion-Type Silicon Ring Modulators

Minkyu Kim, Youngkwan Jo, *Graduate Student Member, IEEE*, Stefan Lischke, Christian Mai, Lars Zimmermann, *Senior Member, IEEE*, and Woo-Young Choi, *Member, IEEE*

***Abstract*— We present a large-signal SPICE model for the depletion-type silicon ring (RM) modulator that includes temperature dependence. The model is based on the temperature-dependent equivalent circuit for the RM and allows easy simulation of RM modulation characteristics in SPICE. The accuracy of the model is verified with the measurement results of 25-Gb/s NRZ modulation at several different temperatures. In addition, simulation of the temperature-dependent transient responses of the RM together with the RM temperature control circuit is demonstrated in the standard IC design environment.**

***Index Terms*— Silicon photonics, ring modulators, equivalent circuit model, SPICE model, temperature dependency.**

I. Introduction

DEPLETION-TYPE Si ring modulators (RMs) attract a great amount of research and development interests because they can provide superior performances for demanding optical interconnect applications with their large modulation bandwidth, small-footprint, and energy-efficient operation [1]–[3]. However, with their resonant characteristics, their performance is highly dependent on temperature. Consequently, a RM temperature controller that can provide the stable and optimal modulation characteristics is necessary for any practical application of Si RMs [4]–[9]. Furthermore, since the performance of the modulator driving electronics are also strongly influenced by temperature, there is a great demand for the capability of temperature-aware electro-photonic co-simulation of the entire transmitter including RM, temperature controller, and driver electronics in the design stage, preferably in the standard IC design environment [10], [11]. Previously, we demonstrated a large-signal SPICE model for the Si RM that allows accurate and computationally-efficient co-simulation of the RM together with the driver electronics in the standard IC design platform [12]. This model, however, did not contain temperature dependence. In this letter, we expand this model by adding temperature dependence. The accuracy of our extended model is verified by comparing the simulated eye diagrams with the measurement results for 25-Gb/s NRZ modulation at several different temperatures. Furthermore, using the model, we demonstrate the capacity of co-simulating temperature-dependent transient responses of the Si RM together with temperature-control (TC) electronics.

This letter is organized as follow. In section II, key parameters that are needed for describing temperature dependency of the RM characteristics are identified, and their values are extracted for a sample Si RM. In Section III, the temperature-dependent large-signal SPICE model for the Si RM is described, and its accuracy is verified with measurement results. Section IV provides the results of electronic-photonic co-simulation in SPICE, in which the transient temperature-dependent modulation characteristics of the RM together with the TC IC are investigated. Section V gives the conclusion. The initial results of this work were reported in [13]. However, this letter provides more detailed explanations as well as simulation and measurement results in the larger temperature range.

II. Temperature-Dependent Si RM Parameters

The key parameters for describing the Si RM modulation characteristics are the effective index of the ring waveguide (n_{eff}), the field ratio after one round-trip in the ring waveguide (α), and the coupling coefficient in the directional coupler between ring and bus waveguides (γ). With these parameters, the RM transmission, T, is given as [14]

$$T = \frac{P_{out}}{P_{in}} = \frac{\alpha^2 - 2\alpha\gamma\cos(\phi) + \gamma^2}{1 - 2\alpha\gamma\cos(\phi) + (\alpha\gamma)^2}, \tag{1}$$

where $\phi = \frac{2\pi n_{eff}}{\lambda} L_{ring}$ with L_{ring} representing the ring circumstance. In order to determine temperature- dependent characteristics of these parameters, transmission characteristics of a sample Si RM are measured at several different temperatures and the results are shown in Fig. 1. The measured Si RM is fabricated in IHP's Si PIC technology. It has 8μm radius and 290nm gap between ring and bus waveguides. As shown in the inset of the figure, the resonance wavelength

Manuscript received April 9, 2021; revised July 13, 2021; accepted July 16, 2021. Date of publication July 27, 2021; date of current version August 2, 2021. This work was supported in part by the Materials and Parts Technology Research Development Program through the Korean Ministry of Trade, Industry, and Energy under Project 10065666 and in part by the National Research Foundation of Korea (NRF) Grant by the Korean Government through the Ministry of Science and ICT (MSIT) under Project 2020R1A2C201508911. *(Corresponding author: Woo-Young Choi.)*

Minkyu Kim was with the High-Speed Circuits and Systems Laboratory, Department of Electrical and Electronics Engineering, Yonsei University, Seoul 03722, South Korea. He is now with IMEC, 3001 Leuven, Belgium.

Youngkwan Jo and Woo-Young Choi are with the High-Speed Circuits and Systems Laboratory, Department of Electrical and Electronics Engineering, Yonsei University, Seoul 03722, South Korea (e-mail: wchoi@yonsei.ac.kr).

Stefan Lischke and Christian Mai are with the IHP Leibniz-Institut für Innovative Mikroelektronik, 15236 Frankfurt (Oder), Germany.

Lars Zimmermann is with the IHP Leibniz-Institut für Innovative Mikroelektronik, 15236 Frankfurt (Oder), Germany, and also with the Department of Electrical Engineering and Computer Science, Technische Universität Berlin, 10587 Berlin, Germany.

Color versions of one or more figures in this letter are available at https://doi.org/10.1109/LPT.2021.3098760.

Digital Object Identifier 10.1109/LPT.2021.3098760

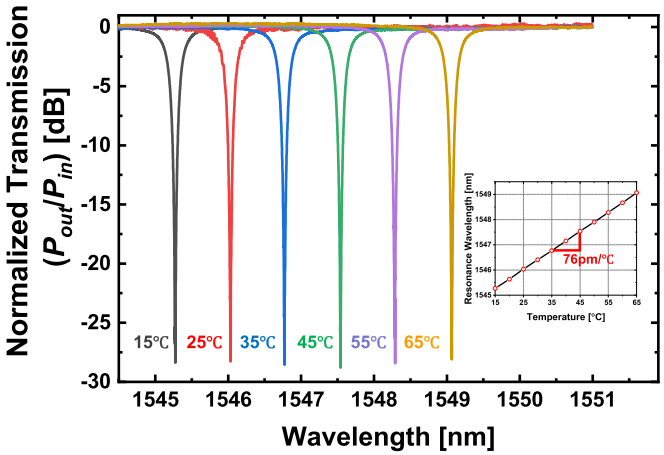

Fig. 1. Measured transmission curves of the fabricated ring modulator with different temperatures and its resonance wavelength.

TABLE I

EXTRACTED KEY PARAMETERS OF Si RM AT DIFFERENT TEMPERATURES (BIAS VOLTAGE = 0 V)

Temperature	n_{eff}	α	γ	R_s [Ω]	C_j [fF]
15 °C	2.613088	0.9804	0.985	-	-
25 °C	2.614376			305.52	12.18
35 °C	2.615619			-	-
45 °C	2.616923			317.9	11.62
55 °C	2.618181			-	-
65 °C	2.619502			323.09	11.39

TABLE II

EXTRACTED KEY PARAMETERS OF Si RM AT DIFFERENT BIAS VOLTAGES (TEMPERATURE = 25°C)

Bias Voltage	n_{eff}	α	γ	R_s [Ω]	C_j [fF]
0 V	2.614376	0.9804	0.985	305.52	12.18
1 V	2.614395	0.9806			8.51
2 V	2.614422	0.9811			6.97

linearly shifts with temperature with the slope of approximately 76 pm/degree. The temperature dependence of n_{eff} can be determined from the resonance condition, $m\lambda_{res} = n_{eff}L_{ring}$, where m is an integer, and the estimated n_{eff} values at different temperatures are shown in Table I. The integer m can be determined with the numerical simulated effective index and measured resonance wavelength. Numerical values for α and γ at any given temperature can be determined by fitting Eq. (1) to the measured transmission characteristics. After performing this fitting process, it is found that there is very little dependence of α and γ on temperature. Consequently, the same α and γ values shown in Table I can be used for the temperature range investigated in this letter. On other hand, α has strong dependence on bias voltages as shown in Table II, and its effect is included in our large-signal model [12].

Electrical characteristics of the Si RM such as series resistance (R_s) and p-n junction capacitance (C_j) also influence the Si RM modulation characteristics. Fig. 2 shows the measured reflection coefficient (S_{11}) of the sample Si RM at different temperatures and voltages. By the equivalent

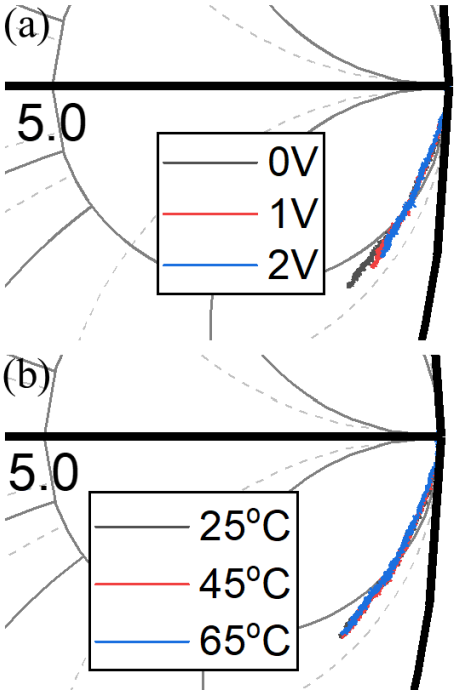

Fig. 2. Measured reflection coefficient (S11) results of RM at (a) different bias voltages with 25°C temperature, and (b) different temperatures with 0V bias voltage.

circuit model [12] fitted to the measured results, junction capacitance and series resistance by voltages can be extracted shown in Table II. As can be seen in Fig.2(b), there is very little change within the temperature range investigated and 3-dB BW variance is near 1% within temperature range as extracted in Table II, which is negligible effect. As a result, there is negligible change in terms of temperature for RC electrical components as well as α and γ, which means the key component for temperature-aware model will be effective index (n_{eff}).

III. LARGE-SIGNAL SPICE MODEL WITH TEMPERATURE DEPENDENCE

The previously reported large-signal SPICE model for the Si RM [12] is based on the small-signal frequency modulation response derived from the RM coupled-mode equations given as [15]

$$\frac{s + (2/\tau_l)}{s^2 + (2/\tau)s + D^2 + (1/\tau^2)}, \tag{2}$$

where D is the difference between the input light wavelength and the resonance wavelength, τ_l and τ are the time-constants due to the ring waveguide loss, and due to the total loss including coupler loss, respectively. τ_l and τ are related to α and γ as [16]

$$\frac{1}{\tau_l} = \frac{(1-\alpha^2)c}{2n_{eff}L_{ring}}, \quad \frac{1}{\tau} = \frac{(2-\alpha^2-\gamma^2)c}{2n_{eff}L_{ring}}. \tag{3}$$

Eq. (2) can be represented by an RLC circuit shown in the right side of Fig. 3(a). The R, L, C values can be obtained by

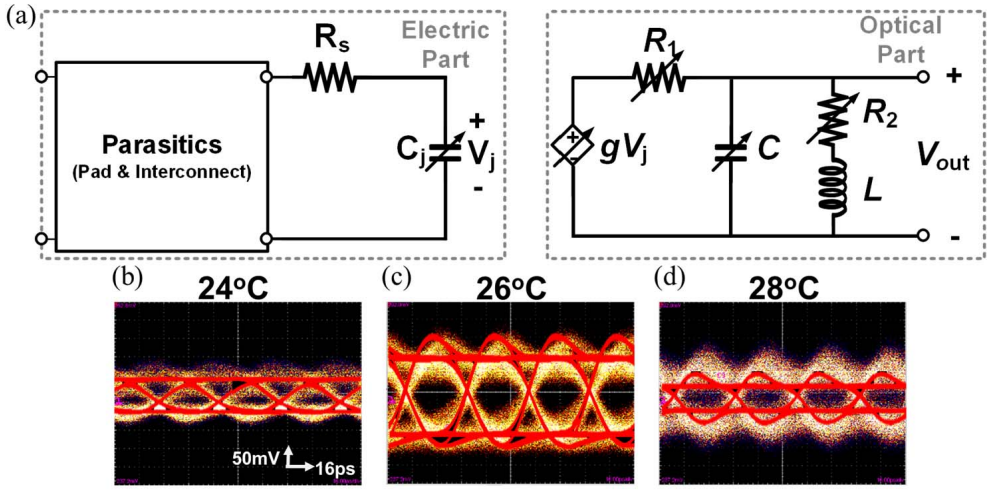

Fig. 3. (a) Equivalent circuit model for depletion-type silicon ring modulator with its temperature dependency and (b-d) model verification by measured (yellow) and simulated (red solid) 25-Gb/s PRBS31 eye-diagrams for different operating temperatures.

matching Eq. (2) to the transfer function of the RLC circuit with τ_1 and τ determined from Eq. (3) using extracted α, γ, n_{eff} values. By employing voltage-dependent R,L,C elements in the equivalent circuit, the small-signal equivalent circuit model can be extended for large-signal emulation of the Si RM modulation behavior [15].

Together with the left-side block representing the RM electrical property, the entire circuit in Fig. 3(a) is the equivalent circuit for the RM modulation characteristics. In this equivalent circuit, variable resistor and capacitors are used since their values depend on the voltage applied to the Si RM. By extracting numerical values for voltage-dependent α, γ, n_{eff} at different temperatures, all the circuit element values in Fig. 3(a) can be determined and, consequently, the entire large-signal Si RM modulation characteristics can be accurately simulated in SPICE. Each circuit element in the optical part of our equivalent circuit does not have any specific physical meaning. The behavior of the entire circuit emulates the small-signal frequency modulation of the RM. Fig. 3(b), (c), (d) show such simulated eye diagrams when the RM is modulated with 25-Gb/s 2^{31}-1 PRBS NRZ input data having 4-$V_{\text{peak-to-peak}}$ swing with the RM input wavelength of 1545.71nm. The measured RM has 3-dB modulation bandwidth of about 20-GHz, DC modulation efficiency of 20 pm/V, and about 7dB insertion loss excluding the coupling loss. For accurate modeling, the electric parasitic components due to bonding pads and on-chip interconnects are also included in the electrical part of the equivalent circuit [12]. Measurement results within a limited temperature range are provided since, due to the strong temperature dependence of RM modulation characteristics, eye diagrams cannot be obtained if the temperature is beyond the range used. For the simulation, the voltage-dependence of RM parameters are modeled with the third-order polynomials within the SPICE simulator.

The real advantage of our model is the ease with which it can be used for transient co-simulation of RMs and electronic circuits such as the temperature controller. The lower part in Fig. 4 shows the block diagram of the RM TC IC fabricated in IHP's BiCMOS platform [7]. This particular TC IC is used

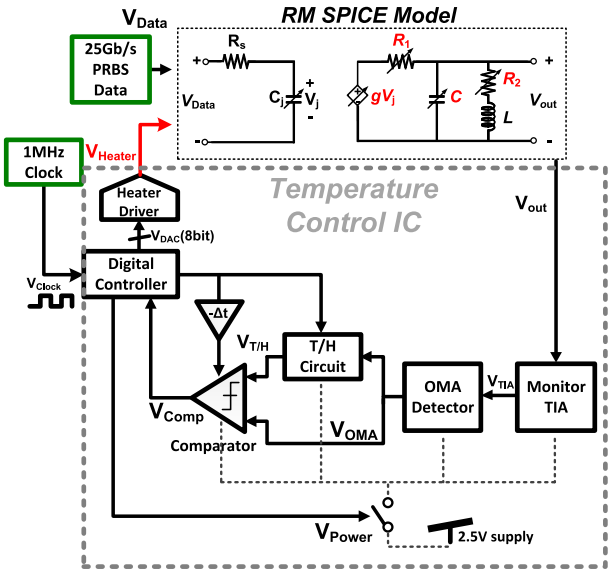

Fig. 4. Block diagram of co-simulation of RM SPICE model and RM TC electronic IC.

since we have the IP but our SPICE RM model can be used with any other TC ICs for Si photonic modulators [4]–[9]. V_{out} in the figure represents the modulated RM output power normalized to the input optical power. The TC IC takes this V_{out} and determines the optical modulation amplitude (OMA). Then, the digital controller within the TC IC determines and maintains V_{Heater} that when applied to the RM on-chip heater provides the optical RM temperature providing the maximum OMA.

Fig. 5 shows the transient co-simulation results for the RM together with the TC IC shown in Fig. 4. For the simulation, the RM is modulated with 25-Gb/s 2^{31}-1 PRBS data. 1-ps resolution is used for the transient simulation. Initially, the TC IC produces linearly increasing V_{Heater} values for the range of about 10 °C, with which the RM temperature is scanned. Due to the RM temperature dependence, different V_{out} and V_{OMA} values are produced during this scanning,

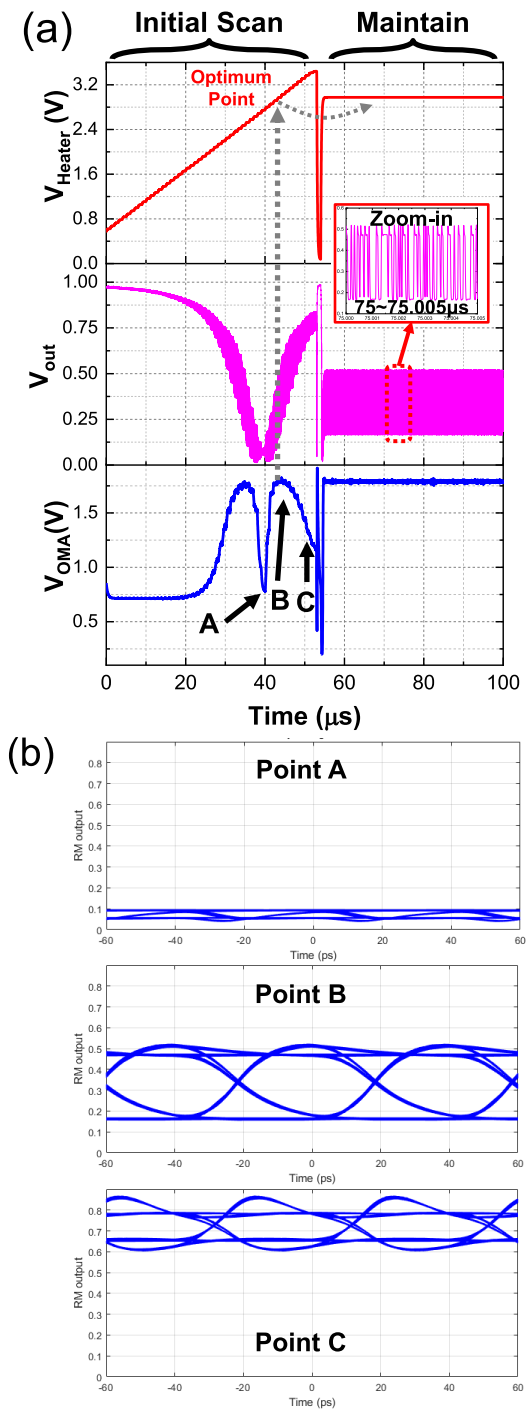

Fig. 5. (a) Simulation results for co-simulation of RM SPICE model and TC IC, and (b) 25Gb/s eye-diagrams for different operating (temperature) points.

as shown in the figure. From the resulting V_{OMA} values, the digital controller selects the largest V_{OMA} (Point B in the figure) corresponding to the largest RM OMA. Then, the digital controller maintains this condition with the feedback control. All these processes are accurately simulated and eye diagrams during any condition can be produced as shown in Fig. 5. This allows the Si photonic transmitter designer the detailed information on the temperature-dependent dynamics of the Si RM and as well as how well the TC IC operates. Such simulation should greatly enhance the design efficiency of the temperature-controlled Si RM as well as the performance of the resulting transmitter.

IV. Conclusion

We present a large-signal SPICE model for the Si RM with temperature awareness. With our model, electro-optic co-simulation of the Si RM with electronic circuits can accurately and efficiently performed in the standard IC design environment. With the model, we demonstrate the temperature-dependent Si RM modulation dynamics together with the TC IC can be successfully simulated. Our model should be of great use for any Si electro-photonic integrated circuits including RMs.

Acknowledgment

The authors are would like to thank IC Design Center (IDEC) for EDA tool support.

References

[1] A. H. Atabaki *et al.*, "Integrating photonics with silicon nanoelectronics for the next generation of systems on a chip," *Nature*, vol. 556, no. 7701, pp. 349–354, Apr. 2018.
[2] X. Chen *et al.*, "The emergence of silicon photonics as a flexible technology platform," *Proc. IEEE*, vol. 106, no. 12, pp. 2101–2116, Dec. 2018.
[3] Y. Shen *et al.*, "Silicon photonics for extreme scale systems," *J. Lightw. Technol.*, vol. 37, no. 2, pp. 245–259, Jan. 15, 2019.
[4] S. Agarwal, M. Ingels, M. Pantouvaki, M. Steyaert, P. Absil, and J. V. Campenhout, "Wavelength locking of a Si ring modulator using an integrated drop-port OMA monitoring circuit," *IEEE J. Solid-State Circuits*, vol. 51, no. 10, pp. 2328–2344, Oct. 2016.
[5] C. Sun *et al.*, "A 45 nm CMOS-SOI monolithic photonics platform with bit-statistics-based resonant microring thermal tuning," *IEEE J. Solid-State Circuits*, vol. 51, no. 4, pp. 893–907, Apr. 2016.
[6] Y. Thonnart *et al.*, "A 10 Gb/s Si-photonic transceiver with 150 μW 120 μs-lock-time digitally supervised analog microring wavelength stabilization for 1Tb/s/mm^2 die-to-die optical networks," in *IEEE Int. Solid-State Circuits Conf. (ISSCC) Dig. Tech. Papers*, Feb. 2018, pp. 350–352.
[7] M.-H. Kim, L. Zimmermann, and W.-Y. Choi, "A temperature controller IC for maximizing Si micro-ring modulator optical modulation amplitude," *J. Lightw. Technol.*, vol. 37, no. 4, pp. 1200–1206, Feb. 15, 2019.
[8] M. Kim *et al.*, "Silicon electronic-photonic integrated 25 Gb/s ring modulator transmitter with a built-in temperature controller," *Photon. Res.*, vol. 9, no. 4, pp. 507–513, Apr. 2021.
[9] H. Li *et al.*, "A 3-D-integrated silicon photonic microring-based 112-Gb/s PAM-4 transmitter with nonlinear equalization and thermal control," *IEEE J. Solid-State Circuits*, vol. 56, no. 1, pp. 19–29, Jan. 2021.
[10] B. Wang *et al.*, "A compact verilog—A model of silicon carrier-injection ring modulators for optical interconnect transceiver circuit design," *J. Lightw. Technol.*, vol. 34, no. 12, pp. 2996–3005, Jun. 15, 2016.
[11] J. Rhim, Y. Ban, B.-M. Yu, J.-M. Lee, and W.-Y. Choi, "Verilog—A behavioral model for resonance-modulated silicon micro-ring modulator," *Opt. Exp.*, vol. 23, no. 7, pp. 8762–8772, 2015.
[12] M. Kim *et al.*, "Large-signal SPICE model for depletion-type silicon ring modulators," *Photon. Res.*, vol. 7, no. 9, p. 948, Sep. 2019.
[13] M. Kim, S. Lischke, C. Mai, L. Zimmermann, and W.-Y. Choi, "An accurate and computationally efficient large-signal SPICE model for depletion-type silicon ring modulators including temperature dependence," in *Proc. Eur. Conf. Opt. Commun. (ECOC)*, Brussels, Belgium, Dec. 2020, pp. 1–3, doi: 10.1109/ECOC48923.2020.9333289.
[14] W. Bogaerts *et al.*, "Silicon microring resonators," *Laser Photon. Rev.*, vol. 6, no. 1, pp. 47–73, Jan. 2012.
[15] Y. Ban, J.-M. Lee, B.-M. Yu, S.-H. Cho, and W.-Y. Choi, "Small-signal frequency responses for Si micro-ring modulators," in *Proc. Opt. Interconnects Conf.*, 2014, vol. 7, no. 1, pp. 47–48.
[16] B. E. Little, S. T. Chu, H. A. Haus, J. Foresi, and J.-P. Laine, "Microring resonator channel dropping filters," *J. Lightw. Technol.*, vol. 15, no. 6, pp. 998–1005, Jun. 1997.